11

Dynamic effects and impact

11.1 Stress waves in solids

So far in this book we have discussed contact problems in which the rate of loading is sufficiently slow for the stresses to be in statical equilibrium with the external loads at all times during the loading cycle. Under impact conditions, on the other hand, the rate of loading is very high and dynamic effects may be important: in rolling and sliding contact at high speed the inertia of the material elements as they 'flow' through the deforming region may influence the stress field. In this chapter we shall examine the influence of inertia forces on a number of contact problems.

Inertia forces are incorporated in the mechanics of deformable solids by the addition in the stress equilibrium equations (2.1) of terms equal to the product of the density of the material ρ and the acceleration of the material element $\partial^2 u/\partial t^2$ at the point in question. When these modified equilibrium equations are combined with the equations of compatibility and the elastic stress-strain relations, solutions for stresses and displacements are obtained which may be interpreted as pulses or waves which travel through the solid with characteristic speeds (see Timoshenko & Goodier, 1951; Kolsky, 1953; or Graff, 1975).

We shall introduce the concept of a stress wave by considering the one-dimensional example of compression waves in a thin elastic rod (see Fig. 11.1). In this simple treatment we shall consider a stress pulse of intensity $-\sigma$ travelling along the rod from left to right with a velocity c_0. In time dt the wave front moves a distance dx ($= c_0\, dt$) and the element, of mass $\rho A\, dx$, acquires a velocity v under the action of the pressure pulse, where ρ is the density of the material and A is the cross-sectional area of the rod. The momentum equation for the element is thus

$$-\sigma A\, dt = (\rho A\, dx)v = \rho A c_0 v\, dt$$

https://doi.org/10.1017/CBO9781139171731.012 Published online by Cambridge University Press

i.e.

$$\sigma = -\rho c_0 v \tag{11.1}$$

The element will have become compressed by du ($= v\,dt$), so that the strain in the element is:

$$-\frac{du}{dx} = -\frac{v}{c_0} = -\frac{\sigma}{E} \tag{11.2}$$

Eliminating σ and v from equations (11.1) and (11.2) gives an expression for the velocity of the pulse:

$$c_0 = (E/\rho)^{1/2} \tag{11.3}$$

which is a characteristic of the material. Since elastic strains are generally small, it is clear from equation (11.2) that the velocity v of particles of the rod is much less than the velocity of the pulse c_0. We note that in a compressive wave, such as we have been considering, the particles move in the same direction as the wave; whereas in a tension wave they move in the opposite direction.

To illuminate our discussion in the next section of the impact of solid bodies, it is instructive now to consider the wave motion set up in a thin elastic rod (Fig. 11.1) fixed at one end and struck on the other by a rigid block of mass M, moving with velocity V. Any tendency of the rod to buckle will be ignored. Immediately after impact the left-hand end of the rod acquires the velocity of the block V and a compression wave propagates along the rod with velocity c_0 given by (11.3). The initial compressive stress in the rod, given by equation (11.1) is $-\rho c_0 V$. The block decelerates under the action of the compressive force in the rod at the interface with the block. The sequence of events then depends upon the mass of the striker M compared with the mass of the rod ρAL.

A light striker is rapidly brought to rest by the compression in the rod; the pressure of the rod on the block decreases as the velocity of the block decreases. There is then a large variation in stress along the rod from $-\rho c_0 V$ at the wave front to a small value at the interface with the block. Meanwhile the pressure

Fig. 11.1. Impact of a rigid mass M on the end of an elastic rod. A compressive wave of intensity $-\sigma$ propagates along the rod with velocity c_0.

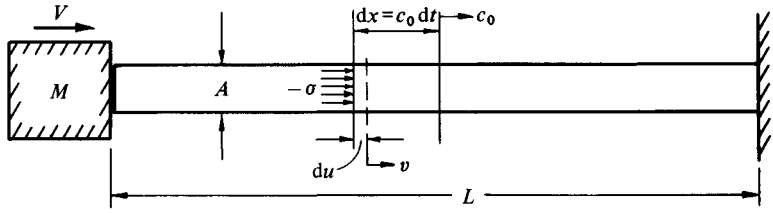

https://doi.org/10.1017/CBO9781139171731.012 Published online by Cambridge University Press

wave is reflected at the fixed end of the rod. When the reflected wave returns to the free end it accelerates the block and is itself partially reflected. Thus the block rebounds from the end of the rod with a velocity less than V and the rod is left in a state of vibration. The maximum stress in the rod as a result of the impact is $\rho c_0 V$, which is independent of M. It occurs first at the instant of impact and again when the reflected wave impinges on the block.

At the other extreme, if the mass of the striker is much larger than that of the rod, the pressure wave is reflected up and down the rod many times before the block is brought to rest. The state of stress in the bar at any instant is approximately uniform throughout its length and the sudden changes in stress associated with the passage of the stress wave in the rod are small compared with the general stress level. The stress in the rod can then be found to a good approximation by ignoring dynamic effects in the rod and treating it as a 'light spring'. The maximum stress in the rod, which occurs at the instant the striker comes to rest, can be found by equating the maximum strain energy stored in the bar to the loss of kinetic energy of the striker, with the result:

$$\sigma_{\max} = V(ME/AL)^{1/2}$$

which does depend upon M and is very different from the previous result. An analysis of a dynamic problem on these lines in which inertia forces in the deforming material are neglected is usually referred to as *quasi-static* since the external dynamic loads are taken to be in 'equilibrium' with a statically determined stress field.

The two extreme cases described above arise when the mass of the striker is either much smaller or much larger than the total mass of the rod; put another way these conditions correspond to a time for the mass to come to rest which is either short or long compared with the time for a stress wave to travel to the end of the rod and back. When these times are similar the behaviour is much more complex. This problem and others involving the longitudinal impact of rods are discussed by Goldsmith (1960) and Johnson (1972).

So far we have assumed perfectly elastic behaviour, but impact stresses are generally high and inelastic deformation plays an important part in practical impacts. For elastic behaviour the stress given by equation (11.1) must be less than the yield stress Y, for which the impact velocity

$$v \leqslant Y/\rho c_0 \tag{11.4}$$

The longitudinal wave speed in steel, given by (11.3), is about 5200 m/s. Taking $Y = 300$ N/mm^2, the maximum impact velocity for elastic deformation is 7.5 m/s. At speeds below this value, elastic hysteresis in the steel causes the elastic waves to attenuate slowly with distance travelled. Above this speed the end of the bar becomes plastically deformed and the elastic wave travelling at c_0 is followed by a slower moving plastic wave.

In extended three-dimensional elastic bodies two types of wave motion are possible: (i) *dilatational* (or pressure) waves in which the material elements fluctuate in volume without shear deformation and (ii) *distortional* (or shear) waves in which the elements distort without change in volume. The speeds of propagation of these waves in isotropic materials are given by:

$$\text{dilatation: } c_1 = \left\{\frac{2(1-\nu)G}{(1-2\nu)\rho}\right\}^{1/2} \tag{11.5}$$

$$\text{distortion: } c_2 = (G/\rho)^{1/2} \tag{11.6}$$

where G is the elastic shear modulus.

For $\nu = 0.25$, $c_1 = \sqrt{3}\, c_2$. If the wave front is planar, which would be approximately so at a large distance from a point source, the motion of the material particles in a dilatational wave is in the direction of propagation of the wave front and the waves are sometimes described as *longitudinal.* In a distortional wave, on the other hand, the particles move at right angles to the direction of propagation of the wave so that the waves are then referred to as *transverse.*

Where the solid body is bounded by a plane or near-planar surface, such as we are concerned with in elastic contact problems, waves known as Rayleigh waves may be propagated along the surface with a velocity

$$c_3 = \alpha c_2 = \alpha(G/\rho)^{1/2} \tag{11.7a}$$

where α is the root of the equation

$$(2-\alpha^2)^4 = 16(1-\alpha^2)(1-\alpha^2 c_2^2/c_1^2) \tag{11.7b}$$

The value of α depends upon Poisson's ratio; for $\nu = 0.25$, $\alpha = 0.919$, and for $\nu = 0.5$, $\alpha = 0.955$, so that the speed of surface waves is just slightly less than that of distortion waves. Values of the wave velocities in a few common solids are given in Table 11.1

11.2 Dynamic loading of an elastic half-space

The starting point for our consideration of the static loading of an elastic half-space in Chapters 2 and 3 was the action of a concentrated force

Table 11.1. *Elastic wave velocities* (m/s)

		Steel	Copper	Aluminium	Glass	Rubber
1-dimensional tens./compr.	c_0	5200	3700	5100	5300	46
Dilatational	c_1	5900	4600	6300	5800	1100
Distortional	c_2	3200	2300	3100	3400	27
Rayleigh	c_3	3000	2100	2900	3100	26

https://doi.org/10.1017/CBO9781139171731.012 Published online by Cambridge University Press

applied normal to the surface. The stresses and deformations due to distributed loads could then be found by superposition. The equivalent problems in dynamic loading are those of a concentrated line or point force P which is (*a*) applied suddenly and then maintained constant - a step - or (*b*) an impulse

$$\hat{P} = \left[\int_0^{\Delta t} P \, dt\right]_{\Delta t \to 0}$$

or (*c*) an harmonically varying force $P = P^* \cos \omega t$. Each of these fundamental solutions can be used to build up a distributed load by superposition with respect to position on the surface and a time-varying pulse $P(t)$ by superposition with respect to time.

The wave motion initiated in a half-space by a step point force has been analysed by Pekeris (1955) and is depicted in Fig. 11.2. Following the application of the load at time $t = 0$, spherical wave fronts of pressure (P) waves and shear (S) waves propagate from the point of application of the load with

Fig. 11.2. Wave motion in an elastic half-space caused by a step load P_0. (*a*) Wave fronts, (*b*) Normal displacement at the surface $z = 0$. ($\nu = \frac{1}{4}$.)

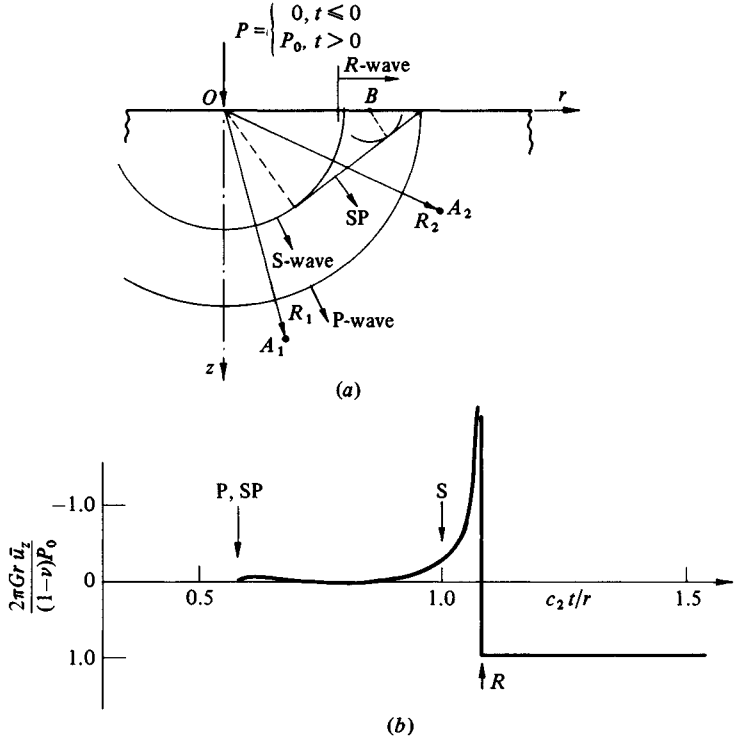

https://doi.org/10.1017/CBO9781139171731.012 Published online by Cambridge University Press

velocities c_1 and c_2. At point A_1 within the solid, distance $R_1 = (r_1^2 + z_1^2)^{1/2}$ from O, the material is unstressed until a time $t = R_1/c_1$, when the P-wave arrives, and it experiences a step radial displacement; at a later time $t = R_1/c_2$, the S-wave arrives imparting a step circumferential displacement. The magnitude of the displacement decreases as $1/R$ and of the stresses as $1/R^2$. The interaction of the P-wave with the free surface of the half-space initiates a weak disturbance - the 'head wave' or SP-wave - which propagates with velocity c_2 as shown in Fig. 11.2(*a*) and which influences slightly the displacements and stresses experienced by a subsurface point such as A_2. The interaction of the S-wave with the free surface gives rise to the Rayleigh wave which we have seen propagates with a velocity c_3 slightly less than the S-wave, and influences points which are on or close to the surface. The time-history of normal displacement $\bar{u}_z$ of points on the surface is shown in Fig. 11.2(*b*). It is evident that the predominant effect is that of the Rayleigh wave which decays as $1/R^{1/2}$, which is more slowly than either P or S waves. After the Rayleigh wave has passed, the surface is left with its static displacement under the action of a steady force P_0, given by equation (3.22*b*).

The effects of an impulsive line load and harmonically varying line and point loads have been analysed in a classic paper by Lamb (1904). We shall consider a point load

$$P(t) = P^* \cos \omega t \tag{11.8}$$

acting normally to the surface at the origin O. In the steady state, the wave system comprises P-waves moving with velocity c_1 and S-waves moving with velocity c_2 on spherical wavefronts centred at O. In addition Rayleigh waves radiate outwards on the surface of the half-space with velocity c_3.

Within the body, at a radial distance R from O which is large compared with the wavelength, the radial displacement u_R is entirely due to the pressure wave and is given by (Lamb, 1904; Miller & Pursey, 1954)

$$u_R = \frac{P^*}{2\pi GR} \frac{\cos\theta\,(\mu^2 - 2\sin^2\theta)}{F_0(\sin\theta)} \cos(\omega t - k_1 R) \tag{11.9a}$$

The transverse displacement u_θ is due to the shear wave and is given by

$$u_\theta = \frac{\mathrm{i}\mu^3 P^*}{2\pi GR} \frac{\sin 2\theta\,(\mu^2 \sin^2\theta - 1)^{1/2}}{F_0(\mu \sin\theta)} \sin(\omega t - k_2 R) \tag{11.9b}$$

In equations (11.9), $\theta = \cos^{-1}(z/R)$, $k_1 = \omega/c_1$, $k_2 = \omega/c_2$,

$$\mu = c_1/c_2 = \{2(1-\nu)/(1-2\nu)\}^{1/2},$$

$$F_0(\xi) = (2\xi^2 - \mu^2)^2 - 4\xi^2(\xi^2 - \mu^2)^{1/2}(\xi^2 - 1)^{1/2}$$

On the surface at a distance r from O, which is again large compared with the wavelength, the displacements $\bar{u}_r$ and $\bar{u}_z$ are due to the Rayleigh wave and are

https://doi.org/10.1017/CBO9781139171731.012 Published online by Cambridge University Press

given by

$$\bar{u}_r = \frac{P^*}{G}\left(\frac{k^3}{2\pi r}\right)^{1/2} F_r(\nu)\sin(\omega t - k_3 r - \pi/4) \tag{11.10a}$$

$$\bar{u}_z = \frac{P^*}{G}\left(\frac{k^3}{2\pi r}\right)^{1/2} F_z(\nu)\cos(\omega t - k_3 r - \pi/4) \tag{11.10b}$$

where $k_3 = \omega/c_3$; $F_r(\nu)$ and $F_z(\nu)$ are functions of Poisson's ratio (see Miller & Pursey, 1954). For $\nu = 0.25$, $F_r(\nu) = 0.125$, $F_z(\nu) = 0.183$.

Equations (11.9) and (11.10) are not accurate close to the origin but, in any case, the displacement and corresponding stresses become infinite at the point of application of a concentrated force (as R and r approach zero). The more realistic situation of a uniform pressure p acting on a circular area of radius a and oscillating with angular frequency ω has been analysed by Miller & Pursey (1954). This is the dynamic equivalent of the static problem discussed in §3.4(*a*). The wave motion at a large distance from the loaded circle (R, $r \gg a$) is the same as for a concentrated force $P = \pi a^2 p$ and the elastic displacements are given by equations (11.9) and (11.10). The mean normal displacement within the contact area $(\bar{u}_z)_m$ is of interest since it determines the 'receptance' of the half-space to an oscillating force. The receptance is defined as the ratio of the mean surface displacement $(\bar{u}_z)_m$ within the loaded area to the total load.† It is a complex quantity: the real part gives the displacement which is in-phase with the applied force; the imaginary part gives the displacement which is $\pi/2$ out-of-phase with the force.

If we write the inverse or reciprocal of the receptance in the form

$$\frac{P}{(\bar{u}_z)_m} = Ga\left\{f_1 \cos\omega t - \left(\frac{\omega a}{c_2}\right) f_2 \sin\omega t\right\} \tag{11.11}$$

it will be recognised as having the same form as the expression for the inverse receptance of a light spring in parallel with a viscous dashpot. The functions f_1 and f_2 depend upon Poisson's ratio and the frequency parameter $(\omega a/c_2)$. Values taken from Miller & Pursey (1954) are shown by the full lines in Fig. 11.3. In the range considered, f_1 and f_2 do not vary much with frequency so that, to a reasonable approximation, the elastic half-space can be modelled by a light spring in parallel with a dashpot. The energy 'dissipated' by the dashpot corresponds to the energy radiated through the half-space by wave motion. The stiffness of the spring may be taken to be independent of frequency and equal to the static stiffness of the half-space given by equation (3.29*a*); the

† An alternative quantity which is commonly used to give the same information is the 'impedance' which is the ratio of the force to the mean velocity of surface points in the loaded area.

https://doi.org/10.1017/CBO9781139171731.012 Published online by Cambridge University Press

spring and dashpot combination has a time constant $T = f_2 a/f_1 c_2 \approx 0.74a/c_2$. In this way the power radiated through the half-space by wave motion can easily be calculated to be ($\nu = 0.25$)

$$\dot{W} = 0.074P^2\omega^2/Gc_2 \tag{11.12}$$

Using equations (11.9) and (11.10) the partition of this energy between the different wave motions has been found by Miller & Pursey (1955). The pressure waves account for 7%, the shear waves for 26% and the surface waves for 67% of the radiated energy. If we note that the pressure and shear waves decay in amplitude (neglecting dissipation) with (distance)$^{-1}$ whilst the surface waves

Fig. 11.3. Receptance functions f_1 and f_2 for an elastic half-space: solid line – uniform pressure on circle radius a; large-dashed line – uniform pressure on strip width $2a$; chain line – uniform pressure on semi-infinite rod; small-dashed line – uniform displacement on circle radius a.

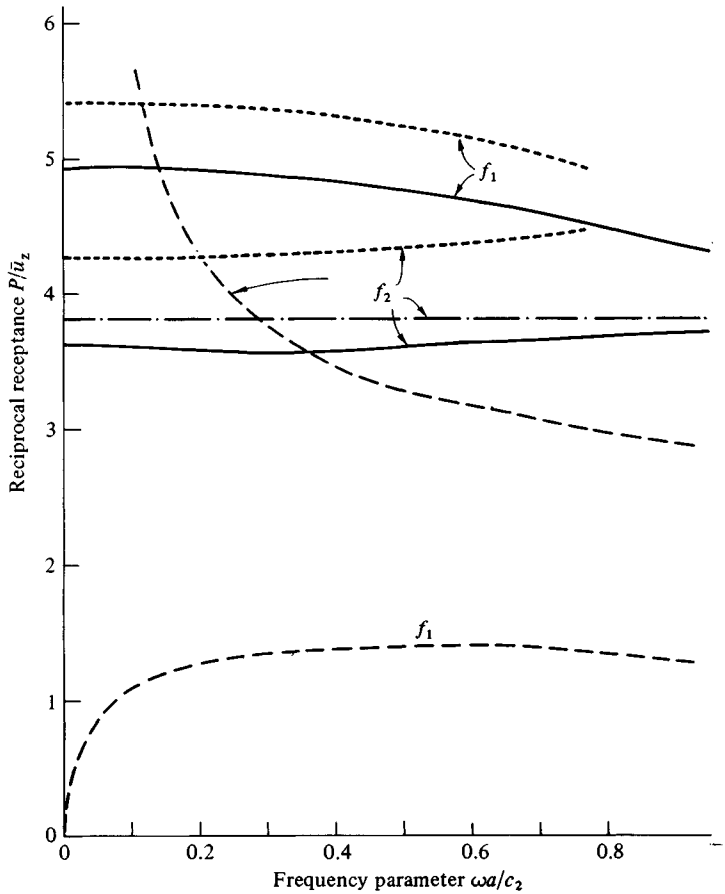

https://doi.org/10.1017/CBO9781139171731.012 Published online by Cambridge University Press

decay with (distance)$^{-1/2}$, it is clear that the predominant effect at some distance from the point of excitation is the surface wave. This explains why earthquakes can be damaging over such a large area.

The spring and dashpot model can be applied to other situations. A semi-infinite thin rod transmits one-dimensional longitudinal waves as described in §1. In view of its infinite length the rod has zero static stiffness in tension and compression. By equation (11.1) the force on the end of the rod is proportional to the *velocity* of the end. Thus under the action of an oscillating force the rod acts like a pure dashpot. The function $f_1 = 0$ and $f_2 = 3.84$. Miller & Pursey (1954) have also considered an elastic half-space loaded two-dimensionally by an oscillating pressure applied to a strip of width $2a$. In this case the functions f_1 and f_2 show larger variations with frequency (Fig. 11.3).

With an interest in the motion transmitted to the ground through the foundation of a vibrating machine, Arnold *et al.* (1955), Robertson (1966) and Gladwell (1968) studied the allied problem of a circular region on the surface of an elastic half-space which is oscillating with a uniform normal displacement. In this case the pressure distribution is not uniform. The receptance functions f_1 and f_2 computed by Gladwell are also plotted in Fig. 11.3. Not surprisingly they do not differ much from the case of a uniform pressure. When $\omega \to 0$, f_1 is given by the static displacement under a circular rigid punch (eq. (3.36)).

In this section we have considered the stresses and displacements in an elastic half-space in response to a sinusoidally oscillating pressure applied to a small circular region on the surface. In the language of the vibration engineer we have determined its linear dynamic response to harmonic excitation. In the next section, dealing with impact, we shall be concerned with the response of the half-space to a single pressure pulse. However, if the variation of the pulse strength with time $P(t)$ is known it can be represented by a continuous spectrum of harmonic excitation $F(\omega)$ by the transformation

$$F(\omega) = \left(\frac{2}{\pi}\right)^{1/2} \int_{-\infty}^{\infty} P(t)\, e^{i\omega t}\, dt \tag{11.13}$$

The response to harmonic excitation at a single frequency ω has been presented in this section. The response to a spectrum of harmonic excitation $F(\omega)$ can be found by superposition, i.e. by integration with respect to ω. In practice, the integration is seldom easy and requires numerical evaluation.

Finally we note that, although our discussion has been restricted to the dynamic response of a half-space to purely normal forces, behaviour which is qualitatively similar arises when tangential forces or couples are applied to the surface. For example, a light circular disc of radius a attached to the surface, in addition to a purely normal oscillation discussed above, can undergo three

other modes of vibration: translation parallel to the surface, rocking about an axis lying in the surface, and twisting about the normal axis. Receptance functions for each of these modes are conveniently summarised by Gladwell (1968).

11.3 Contact resonance

In the previous section we saw that an elastic half-space responds to an oscillating force applied to the surface like a spring in parallel with a dashpot. If now a body of mass m is brought into contact with the half-space the resulting system comprises a mass, spring and dashpot, which might be expected to have a characteristic frequency of vibration and to exhibit resonance when subjected to an oscillating force.

We shall consider first the case of a rigid mass attached to the half-space over a fixed circular area of radius a. This is the problem investigated by Arnold *et al.* (1955). It has obvious application to ground vibrations excited by heavy machinery and also the vibration of buildings excited by earth tremors (Richart *et al.*, 1970). For motion normal to the surface, receptance of the half-space is given by (11.11), so that, denoting the displacement of the mass by $\bar{u}_z$, the equation of motion of the system when excited by an oscillating force $P\cos\omega t$ is:

$$m\ddot{\bar{u}}_z + (Ga^2 f_2/c_2)\dot{\bar{u}}_z + Gaf_1\bar{u}_z = P\cos\omega t \tag{11.14}$$

The frequency of free vibrations is $\omega_0(1-\zeta^2)^{1/2}$, where the undamped natural frequency ω_0 is given by

$$\omega_0^2 = Gaf_1/m \tag{11.15a}$$

and the damping factor ζ by

$$\zeta = \tfrac{1}{2}(f_2/f_1)(\omega_0 a/c_2) = \tfrac{1}{2}(f_2/f_1^{1/2})(\rho a^3/m)^{1/2} \tag{11.15b}$$

A sharp resonance peak will be obtained if $\zeta \ll 1$. Now $\frac{1}{2}(f_2/f_1^{1/2}) \approx 1$, so that the damping factor due to wave propagation is small if the mass of the attached body is large compared with the mass of a cube of the half-space material of side a. In this case the resonant frequency is very nearly equal to ω_0, given by equation (11.15a). Resonance curves for different values of $(\rho a^3/m)$ are plotted for the different modes of vibration in Arnold *et al.* (1955).

We shall turn now to the situation where two non-conforming bodies are pressed into contact by a steady force P_0 and then subjected to an oscillating force $\Delta P\cos\omega t$. As in static contact stress theory we take the size of the contact area to be small compared with the dimensions of either body, in which case it follows that the parameter $(\rho a^3/m)$ must be small for both bodies. This means that the vibrational energy absorbed by wave motion is small. Hence, for either body, the damping term in equation (11.14) is negligible

https://doi.org/10.1017/CBO9781139171731.012 Published online by Cambridge University Press

and the elastic stiffness term is given by the static stiffness $Gaf_1(\omega = 0)$. Since both bodies are deformable the effective 'contact spring' between them is the series combination of the stiffness of each body regarded as an elastic half-space. The mass of each body may be considered to be concentrated at its centroid. It is then a simple matter to calculate their frequency of *contact resonance.*

The frequency of contact resonance may be approached from another point of view. The relation between normal contact force and relative displacement of the two bodies is given by equation (4.23) for a circular contact area and by equation (4.26*c*) for an elliptical contact. Both may be written

$$P = K\delta^{3/2} \tag{11.16}$$

where the constant K depends upon the geometry and elastic constants of the two bodies. This relationship is nonlinear, but for small variations ΔP about a mean load P_0, the effective stiffness is given by

$$s = \frac{dP}{d\delta} = \tfrac{3}{2}(K^2 P_0)^{1/3} \tag{11.17}$$

If the bodies have masses m_1 and m_2 and are freely supported, the frequency of contact resonance is given by

$$\omega_0{}^2 = \frac{s(m_1 + m_2)}{m_1 m_2} \tag{11.18}$$

As we have seen, the effective damping arising from wave propagation is negligible but in practice there will be some damping due to elastic hysteresis as described in §6.4.

At resonance, when large amplitudes of vibration occur, the behaviour is influenced by the nonlinear form of the force-displacement relation (11.16). Under a constant mean load P_0 the effective stiffness decreases with amplitude, so that the resonance curve takes on the 'bent' form associated with a 'softening' spring (see Den Hartog, 1956). Thus the frequency at maximum amplitude is less than the natural frequency given by equation (11.18), which assumes small amplitudes. Under severe resonant conditions the two bodies may bounce out of contact for part of the cycle.

We have seen how contact resonance arises in response to an oscillating force. It also occurs in rolling contact in response to periodic irregularities in the profiles of the rolling surfaces (see Gray & Johnson, 1972). The vibration response of two discs rolling with velocity V to sinusoidal corrugations of wavelength λ on the surface of one of them is shown in Fig. 11.4. With the smaller corrugation the amplitude of vibration does not exceed the static compression, so that the surfaces are in continuous contact. A conventional resonance curve

is obtained. With the larger corrugation the discs bounce out of contact at resonance and the resonance curve exhibits the 'jump' which is a feature of a highly nonlinear system.

11.4 Elastic impact

The classical theory of impact between frictionless elastic bodies is due to Hertz and follows directly from his statical theory of elastic contact (Chapter 4). The theory is quasi-static in the sense that the deformation is assumed to be restricted to the vicinity of the contact area and to be given by the statical theory: elastic wave motion in the bodies is ignored and the total mass of each body is assumed to be moving at any instant with the velocity of its centre of mass. The impact may be visualised, therefore, as the collision of two rigid railway trucks equipped with light spring buffers; the deformation is taken to be concentrated in the springs, whose inertia is neglected, and the trucks move as rigid bodies. The validity of these assumptions will be examined subsequently.

(a) Collinear impact of spheres

The two elastic spheres, of mass m_1 and m_2, shown in Fig. 11.5, are moving with velocities v_{z1} and v_{z2} along their line of centres when they collide at O. We shall begin by considering collinear impact in which $v_{x1} = v_{x2} = \omega_{y1} =$

Fig. 11.4. Contact resonance curves for rolling discs with one corrugated surface. Corrugation amplitude/static compression: circle ~ 0.30; cross ~ 0.55.

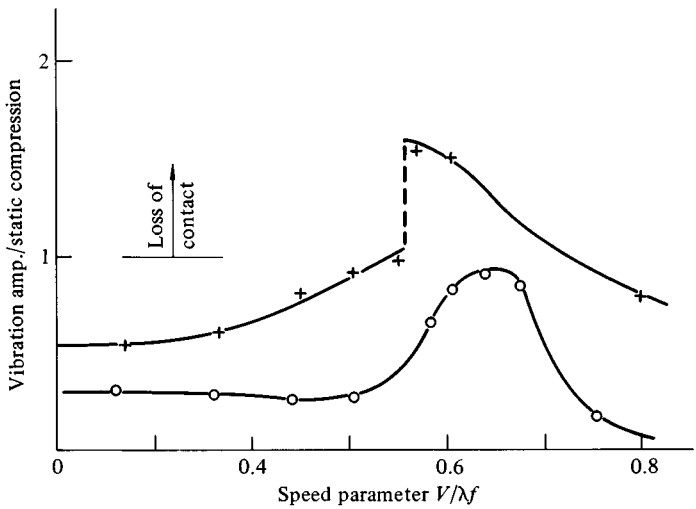

https://doi.org/10.1017/CBO9781139171731.012 Published online by Cambridge University Press

$\omega_{y2} = 0$. During impact, due to elastic deformation, their centres approach each other by a displacement δ_z. Their relative velocity is $v_{z2} - v_{z1} = \mathrm{d}\delta_z/\mathrm{d}t$ and the force between them at any instant is $P(t)$. Now

$$P = m_1 \frac{\mathrm{d}v_{z1}}{\mathrm{d}t} = -m_2 \frac{\mathrm{d}v_{z2}}{\mathrm{d}t}$$

hence

$$-\frac{m_1 + m_2}{m_1 m_2} P = \frac{\mathrm{d}}{\mathrm{d}t}(v_{z2} - v_{z1}) = \frac{\mathrm{d}^2\delta_z}{\mathrm{d}t^2} \tag{11.19}$$

The relationship between P and δ_z is now taken to be that for a static elastic contact given by equation (4.23), i.e.

$$P = (4/3)R^{1/2}E^*\delta_z^{3/2} = K\delta_z^{3/2} \tag{11.20}$$

where $1/R = 1/R_1 + 1/R_2$ and $1/E^* = (1-\nu_1^2)/E_1 + (1-\nu_2^2)/E$. Writing $1/m$ for $(1/m_1 + 1/m_2)$ we get

$$m\frac{\mathrm{d}^2\delta_z}{\mathrm{d}t^2} = -K\delta_z^{3/2} \tag{11.21}$$

Integrating with respect to δ_z gives

$$\tfrac{1}{2}\left\{V_z^2 - \left(\frac{\mathrm{d}\delta_z}{\mathrm{d}t}\right)^2\right\} = \tfrac{2}{5}\frac{K}{m}\delta_z^{5/2}$$

Fig. 11.5

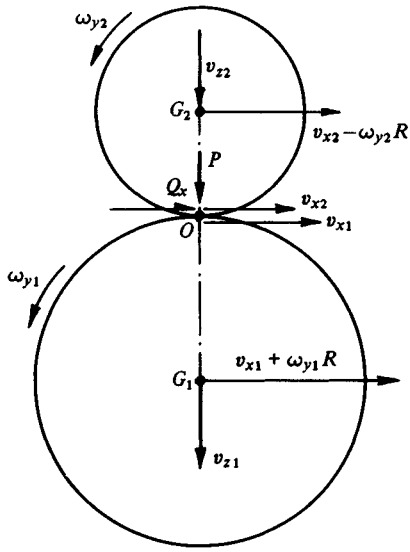

https://doi.org/10.1017/CBO9781139171731.012 Published online by Cambridge University Press

where $V_z = (v_{z2} - v_{z1})_{t=0}$ is the velocity of approach. At the maximum compression δ_z^*, $\mathrm{d}\delta_z/\mathrm{d}t = 0$, which gives

$$\delta_z^* = \left(\frac{5mV_z^2}{4K}\right)^{2/5} = \left(\frac{15mV_z^2}{16R^{1/2}E^*}\right)^{2/5} \tag{11.22}$$

The compression–time curve is found by a second integration, thus

$$t = \frac{\delta_z^*}{V_z}\int \frac{\mathrm{d}(\delta_z/\delta_z^*)}{\{1-(\delta_z/\delta_z^*)^{5/2}\}^{1/2}} \tag{11.23}$$

This integral has been evaluated numerically by Deresiewicz (1968) and converted into a force–time curve in Fig. 11.6. After the instant of maximum compression t^*, the spheres expand again. Since they are perfectly elastic and frictionless, and the energy absorbed in wave motion is neglected, the deformation is perfectly reversible. The total time of impact T_c is, therefore, given by

$$T_c = 2t^* = \frac{2\delta_z^*}{V_z}\int_0^1 \frac{\mathrm{d}(\delta_z/\delta_z^*)}{\{1-(\delta_z/\delta_z^*)^{5/2}\}^{1/2}} = 2.94\delta_z^*/V_z$$
$$= 2.87(m^2/RE^{*2}V_z)^{1/5} \tag{11.24}$$

The above analysis applies to the contact of spheres or to bodies which make elastic contact over a circular area. It can be adapted to bodies having general curved profiles by taking the parameter K in the static compression law from equation (4.26*c*) for the approach of two general bodies. The quasi-static impact of a rigid cone with an elastic half-space has been analysed by Graham (1973).

We can now examine the assumption on which the Hertz theory of impact is based: that the deformation is quasi-static. In §1, when discussing the impact of a thin rod, it was argued that the deformation in the rod would be quasi-

Fig. 11.6. Variation of compression δ_z and force P with time during a Hertz impact. Broken line – sin $(\pi t/2t^*)$.

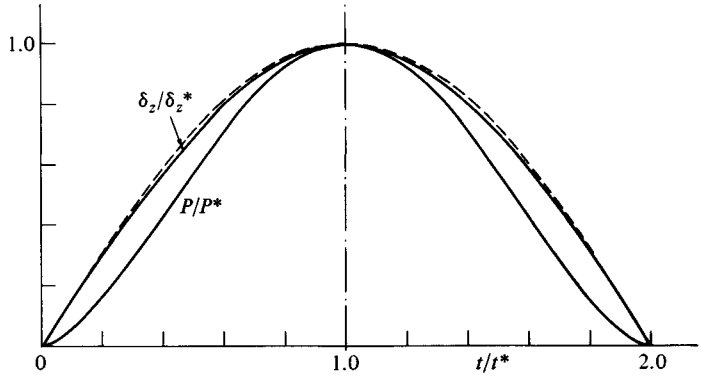

https://doi.org/10.1017/CBO9781139171731.012 Published online by Cambridge University Press

static if the duration of the impact was long enough to permit stress waves to traverse the length of the rod many times. Love (1952) suggested that the same criterion applies in this case. For like spheres, the time for a longitudinal wave to travel two ball diameters is $4R/c_0$. The time of impact, given by equation (11.24), can be expressed as $5.6\,(R^5/c_0{}^4V_z)^{1/5}$, so that the ratio of contact time to wave time $\approx(V_z/c_0)^{1/5}$. According to Love's frequently quoted criterion this quantity should be much less than unity for a quasi-static analysis of impact to be valid.

However, it now appears that Love's criterion, at least in the form stated, is not the appropriate one for three-dimensional colliding bodies. It clearly leads to logical difficulties when one of the bodies is large so that no reflected waves return to the point of impact! We shall now outline an alternative approach due to Hunter (1956), based on the work described in the last section. There it was shown that the dynamic response of an elastic half-space could be found with good approximation by regarding the half-space as an elastic spring in parallel with a dashpot; the energy 'absorbed' by the dashpot accounting for the energy radiated through the half-space by wave motion. Provided the time constant of the system is short compared with the period of the force pulse applied to the system, the force variation during the impact will be controlled largely by the spring, i.e. in a quasi-static manner, and the energy absorbed by the dashpot will be a small fraction of the total energy of impact. We will now find the condition for this to be so.

The force–time variation for a quasi-static elastic impact is given by equations (11.20) and (11.23) and is plotted in Fig. 11.6. It is not an explicit relationship but it is apparent from the figure that it can be approximated by

$$P(t) = P^* \sin \omega t = P^* \sin (\pi t/2t^*), \quad 0 \leqslant t \leqslant 2t^* \tag{11.25}$$

The spring–dashpot model of an elastic half-space has spring stiffness $s(\approx 5Ga)$ and time constant $T \approx 0.74a/c_2 \approx 1.2a/c_0$. When such a system is subjected to the force pulse expressed by equation (11.25), the energy absorbed by the dashpot is small and the response is dominated by the spring if the relaxation time T is short compared with the period of the pulse $2t^*$. If we now take a to be constant and equal to a^* the ratio of times may be written

$$\frac{T}{2t^*} \approx 0.4\,\frac{a^*V_z}{\delta_z^* c_0} = 0.4\,\frac{RV_z}{a^* c_0} \tag{11.26}$$

For quasi-static conditions to be approached this ratio must be much less than unity. For comparison with Love's criterion we consider two like spheres where $m_1 = m_2 = (4/3)\pi\rho R_1{}^3$ and $R = R_1/2$. Equation (11.26) then reduces to

$$T/2t^* \approx 0.3(V_z/c_0)^{3/5} \tag{11.27}$$

https://doi.org/10.1017/CBO9781139171731.012 Published online by Cambridge University Press

This is a much less restrictive condition than that put forward by Love: $T/2t^*$ is less than 1% provided $V_z < 0.002c_0$. As we shall see, however, a more severe restriction is placed on the velocity of impact for the above theory to be valid by the fact that most real materials cease to deform elastically at impact speeds very much less than those possible under the criterion of (11.27).

Although the impact of elastic spheres at practical speeds is virtually quasi-static, Thompson & Robinson (1977) have drawn attention to the behaviour immediately following first contact. Under quasi-static conditions the contact radius a is related to the indentation δ_z by $a^2 = \delta_z R$, so that a grows at a rate $\dot{a} = \dot{\delta}_z R/2a$, where $\dot{\delta}_z$ approximately equals the velocity of impact V_z. Thus, at first contact when a is vanishingly small, $\dot{a}$ can exceed the velocity with which elastic waves propagate on the surface. It turns out, however, that this so-called 'super-seismic phase' occupies a fraction of the total contact time of order V_z/c_1 which is insignificant.

(b) Oblique impact of spheres

If the spheres in Fig. 11.5 have a general coplanar motion then tangential velocities at the point of impact v_x and angular velocities ω_y are introduced. With frictionless surfaces the tangential and rotational motion is undisturbed by the impact. With friction, on the other hand, tangential tractions arise at the interface which influence the motion in an involved way. Denoting the resultant friction force by Q_x, the linear momentum in the tangential direction gives

$$Q_x = m_1 \frac{\mathrm{d}}{\mathrm{d}t}(v_{x1} + \omega_{y1}R_1) = -m_2 \frac{\mathrm{d}}{\mathrm{d}t}(v_{x2} - \omega_{y2}R_2) \tag{11.28}$$

Now the moment of momentum of each sphere about the axis Oy is conserved, i.e.

$$\frac{\mathrm{d}}{\mathrm{d}t}\{m_1 v_{x1}R_1 + m_1(R_1^2 + k_1^2)\omega_{y1}\}$$

$$= \frac{\mathrm{d}}{\mathrm{d}t}\{-m_2 v_{x2}R_2 + m_2(R_2^2 + k_2^2)\omega_{y2}\} = 0 \tag{11.29}$$

where k_1 and k_2 are radii of gyration of the spheres about their centres of mass. Eliminating ω_{y1} and ω_{y2} from (11.28) and (11.29) gives

$$Q_x = \frac{m_1}{1 + R_1^2/k_1^2}\frac{\mathrm{d}v_{x1}}{\mathrm{d}t} = -\frac{m_2}{1 + R_2^2/k_2^2}\frac{\mathrm{d}v_{x2}}{\mathrm{d}t} \tag{11.30}$$

Writing $m_i/(1 + R_i^2/k_i^2) = m_i^*$ and $1/m^* = 1/m_1^* + 1/m_2^*$ we get

$$\frac{1}{m^*}Q_x = \frac{\mathrm{d}}{\mathrm{d}t}(v_{x1} - v_{x2}) = \frac{\mathrm{d}^2\delta_x}{\mathrm{d}t^2} \tag{11.31}$$

https://doi.org/10.1017/CBO9781139171731.012 Published online by Cambridge University Press

where δ_x is the tangential elastic displacement between the two spheres at the point of contact. This equation governs tangential deformation at the contact in the way equation (11.19) governs normal compression. Deformation under the action of tangential forces, however, is complicated by micro-slip. If Q_x reaches its limiting value $\pm\mu P$ the surfaces will slip completely but if $Q_x < |\mu P|$ there may be no slip, but in general an annulus of micro-slip would be expected at the edge of the contact area where the pressure is low. The variations of tangential traction and micro-slip arising from simultaneous variations in tangential and normal forces have been studied by Mindlin & Deresiewicz and are discussed briefly in §7.3. The traction at any instant depends not only upon the values of P and Q, but upon the history of P and Q. This approach has been applied to oblique impact by Maw *et al.* (1976, 1981). The tangential tractions do not affect the normal motion if the materials of the two bodies are elastically similar (i.e. β as defined by eq. (5.3) is zero). However, we have seen in §5.4 that, even for dissimilar materials, the effect is small and may reasonably be neglected. The variation of contact size and contact pressure throughout the impact are thus given by the Hertz theory of impact, independently of friction forces.

The variations of tangential traction and micro-slip throughout the impact have been calculated step by step for different incident conditions. The elastic constants of the two bodies enter the calculation through the ratio of the tangential to normal compliance of a circular contact (see eqs. (7.43) and (7.44)). We define the stiffness ratio κ by

$$\frac{1}{\kappa} \equiv \frac{\dfrac{1-\nu_1/2}{G_1} + \dfrac{1-\nu_2/2}{G_2}}{\dfrac{1-\nu_1}{G_1} + \dfrac{1-\nu_2}{G_2}} \tag{11.32}$$

Thus κ is a material constant close to unity: for similar materials and $\nu = 0.3$, $\kappa = 0.824$. The incident conditions are specified by the non-dimensional parameter $\psi \equiv \kappa V_x/\mu V_z$ where $V_x = (v_{x1} - v_{x2})_{t=0}$ is the tangential velocity of approach before impact. Note that $\tan^{-1}(V_x/V_z)$ is the angle of incidence with which the surfaces approach each other at O. The behaviour during the impact depends upon a second parameter $\chi = \kappa m/2m^*$. For similar homogeneous spheres, with $\nu = 0.3$, $\chi = 1.44$. The variation in Q_x throughout the impact is shown in Fig. 11.7 for different incident conditions. For angles of incidence which are small compared with the angle of friction ($\psi \leqslant 1$) there is no slip at the start of the impact. With larger angles of incidence ($1 < \psi < 4\chi - 1$) the impact starts and finishes with complete slip; in between there is partial slip. At sufficiently high incidence ($\psi \geqslant 4\chi - 1$) sliding takes place throughout the complete time of impact.

https://doi.org/10.1017/CBO9781139171731.012 Published online by Cambridge University Press

Provided that the angle of incidence is not too large it is clear from Fig. 11.7 that the tangential force Q_x undergoes a reversal during the impact, whereas the normal force completes a half cycle only. In the last section we saw that two bodies in contact had a frequency of 'contact resonance' determined by the normal contact stiffness and their masses (eq. (11.18)). A similar behaviour would be expected in tangential motion. The ratio of the tangential to normal frequencies of contact resonance will be

$$\omega_t/\omega_n = (\kappa m/m^*)^{1/2} = (2\chi)^{1/2} \tag{11.33}$$

For solid spheres $\omega_t/\omega_n = 1.7$ which implies that the tangential force almost completes a full cycle during the time when the normal force goes through half a cycle.

The negative tangential force towards the end of the impact is responsible for a negative tangential rebound. Expressing the rebound velocity V_x' by the rebound parameter $\psi' = \kappa V_x'/\mu V_z$, the rebound conditions are plotted as a function of the incident parameter ψ in Fig. 11.8. The tangential rebound velocity V_x' is found to be mainly negative except when $\psi > 4\chi$. The classical rigid body theory of impact, which ignores contact deformation, predicts that the tangential rebound velocity V_x' is either positive, if slipping is continuous, or zero, if slipping ceases during the contact, as shown by the broken lines in Fig. 11.8. The negative tangential rebound velocities predicted in Fig. 11.8 have been substantiated by experiment (see Maw *et al.*, 1981). They are most

Fig. 11.7. Oblique impact of homogeneous solid spheres: the variation of tangential force throughout the impact. ($\nu = 0.3$, $\chi = 1.44$.)

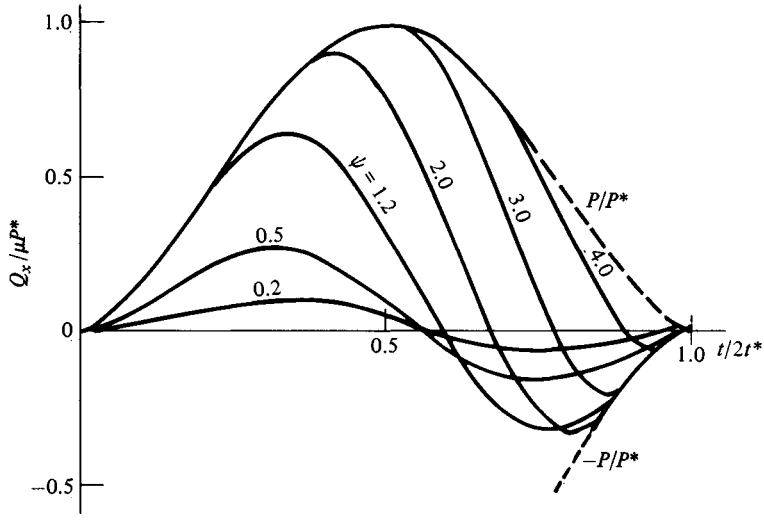

https://doi.org/10.1017/CBO9781139171731.012 Published online by Cambridge University Press

Fig. 11.8. Tangential velocities of incidence and rebound in the oblique impact of homogeneous solid spheres. Broken line – rigid body theory. A: $\nu = 0.3$, B: $\nu = 0.5$.

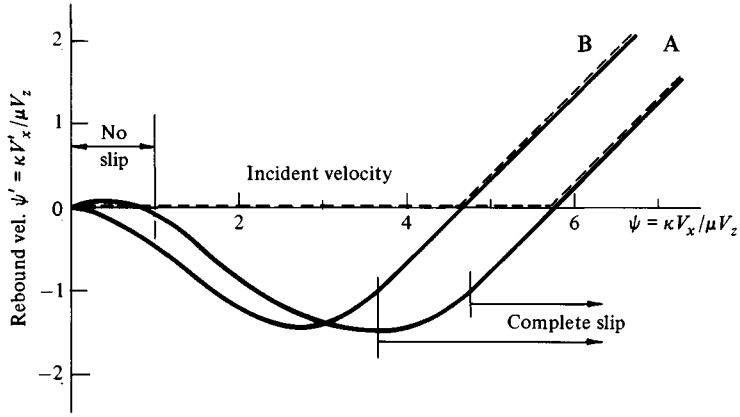

likely to arise when the coefficient of friction is large, for example, with dry rubber surfaces.

(c) Wave motion due to impact

Although the fraction of the impact energy which is radiated as elastic waves is generally very small, in some applications such as seismology it may be important. Tsai & Kolsky (1967) dropped steel balls onto a large block of glass under conditions of elastic impact and measured the radial strain in the surface waves. The variation of strain with time at a particular radial position is shown in Fig. 11.9. An analysis was made along the following lines. The force-time characteristic of Hertzian impact (Fig. 11.6) was assumed to apply and was

Fig. 11.9. Surface wave on a glass block produced by impact of a steel sphere (Tsai & Kolsky, 1967). A – circles joined by dashes – approximation calculation (1967); B – broken line – improved calculation (Tsai, 1968). Solid line – experimental.

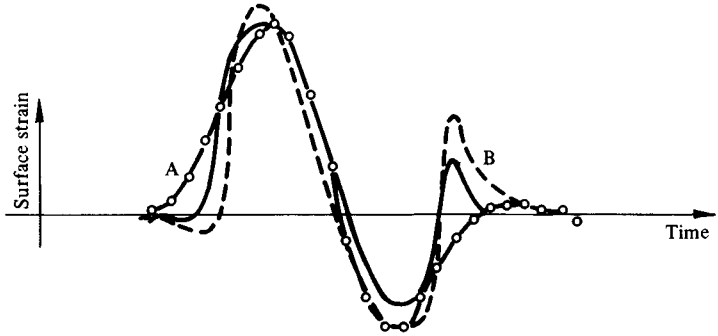

https://doi.org/10.1017/CBO9781139171731.012 Published online by Cambridge University Press

transformed into a continuous spectrum of harmonically varying forces $F(\omega)$, according to equation (11.13). The radial surface displacement $\bar{u}_r$ due to a single frequency of excitation is given by equation (11.10*a*). By substituting the force spectrum $F(\omega)$ for P, integrating with respect to ω and differentiating with respect to r, the time variation of radial strain $\partial \bar{u}_r/\partial r$ due to the impact pulse is obtained. The result of these calculations is shown by Curve A in Fig. 11.9. The agreement with the measured strains is fairly satisfactory. A refined analysis was then made by Tsai (1968) using the more exact expressions for radial displacement given by Miller & Pursey (1954) and taking into account the non-uniform pressure distribution and the variation in contact radius a during the impact. The result is shown by Curve B. The refinements in the analysis do not make a major difference to the result, but they do appear to account for the sharp secondary peak in the measured strain pulse.

More exact dynamic analyses of elastic impact have been made by Tsai (1971) for spherical bodies and by Bedding & Willis (1973) for the penetration of an elastic half-space by a rigid wedge and cone.

The discussion in this section so far has been concerned with collisions between compact bodies, in which stress wave effects account for only a small fraction of the energy of impact and do not influence the local deformation significantly. If one or both of the bodies is slender this conclusion no longer applies.

Let us return to the example of a thin rod, discussed in §1, this time struck on its end by a sphere moving with velocity V. The three-dimensional state of stress at the end of the rod demands some degree of approximation. A convenient approach is to choose a point H, just inside the end of the rod (Fig. 11.10(*a*)),

Fig. 11.10. (*a*) Impact of a sphere on the end of a slender rod; (*b*) Spring-dashpot model.

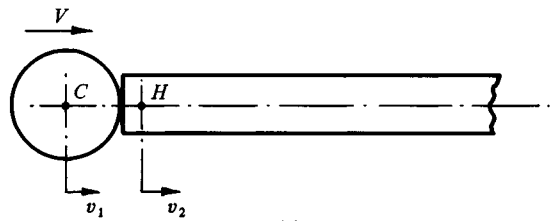

(*a*)

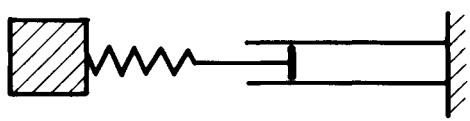

(*b*)

https://doi.org/10.1017/CBO9781139171731.012 Published online by Cambridge University Press

and assume that quasi-static deformation due to the impact takes place to the left of H and that one-dimensional elastic wave propagation takes place to the right of H. The choice of the location of H is somewhat arbitrary, but for most purposes it can be regarded as being adjacent to the end of the rod. If $P(t)$ is the contact force during impact, the momentum equation for the sphere gives the velocity of its centre C to be

$$v_1 = V - \frac{1}{m}\int_0^t P(t)\,\mathrm{d}t \tag{11.34}$$

where m is the mass of the sphere. For the rod, from equation (11.1), the velocity of H is given by

$$v_2 = \frac{1}{A\rho c_0} P(t) \tag{11.35}$$

The approach δ_z of the centre of the sphere C and the point H is given by

$$\delta_z = \int_0^t (v_1 - v_2)\,\mathrm{d}t = Vt - \frac{1}{m}\int_0^t \mathrm{d}t \int_0^t P(t)\,\mathrm{d}t - \frac{1}{A\rho c_0}\int_0^t P(t)\,\mathrm{d}t \tag{11.36}$$

The system can be modelled by a nonlinear spring representing the contact deformation in series with a dashpot which represents the wave motion in the rod (Fig. 11.10(*b*)). If the contact force-compression law is specified, for example by equation (11.20) for an elastic impact, equation (11.36) can be solved numerically to find the force-time history $P(t)$ and the dynamic stresses set up in the rod. Alternatively, if the dynamic strains in the rod are measured, equation (11.36) can be used to determine the force-deformation law at the point of impact (see Crook, 1952). For this technique to be satisfactory the impact must be complete before reflected waves in the rod return to the impact end, which requires the mass of the striker not to be too large compared with the total mass of the rod. At the other extreme, if the striker mass is too small v_2, given by (11.35), becomes negligible compared with v_1 and the rod behaves like a half-space. Davies (1948) has shown this state of affairs arises when the diameter of the sphere is less than half the diameter of the rod.

The approach outlined above can be applied to the longitudinal impact of two rods with rounded ends. A similar situation arises in the transverse impact of a beam by a striker; the local force-compression behaviour is determined by quasi-static considerations, but appreciable energy is transferred into bending vibrations of the beam (see Goldsmith, 1960; or Johnson, 1972).

11.5 Inelastic impact†

(a) Onset of yield

The Hertz theory of elastic impact has been presented in the foregoing section. An elastic-plastic material will reach the limit of elastic behaviour at a point beneath the surface when the maximum contact pressure p_0 at the instant of maximum compression reaches the value $1.60Y$, given by equation (6.9), where Y is the yield stress of the softer body. The maximum value p_0^* during elastic impact can be obtained by using equations (11.20) and (11.22) from which

$$p_0^* = \frac{3}{2\pi}\left(\frac{4E^*}{3R^{3/4}}\right)^{4/5} (\tfrac{5}{4}mV^2)^{1/5} \tag{11.37}$$

where $1/m = 1/m_1 + 1/m_2$, $1/R = 1/R_1 + 1/R_2$ and V is the relative velocity at impact.‡ Substituting the critical value of p_0 gives an expression for the velocity V_Y necessary to cause yielding:

$$\tfrac{1}{2}mV_Y^2 \approx 53R^3 Y^5/E^{*4} \tag{11.38}$$

In the case of a uniform sphere striking the plane surface of a large body, equation (11.38) reduces to

$$\frac{\rho V_Y^2}{Y} = 26(Y/E^*)^4 \tag{11.39}$$

where ρ is the density of the sphere. The impact velocity to cause yield in metal surfaces is very small; for a hard steel sphere striking a medium hard steel ($Y = 1000\ \mathrm{N/mm^2}$), $V_Y \approx 0.14$ m/s. It is clear that most impacts between metallic bodies involve some plastic deformation.

(b) Plastic impact at moderate speeds

In the last section we justified a quasi-static approach to finding the contact stresses during elastic impact, provided the impact velocity is small compared with the elastic wave speed. This condition remains valid when plastic deformation occurs, since the effect of plastic flow is to reduce the intensity of the contact pressure pulse and thereby to diminish the energy converted into elastic wave motion. At moderate impact velocities (up to 500 m/s, say) we can make use of our knowledge of inelastic contact stresses under static conditions (from Chapter 6) to investigate impact behaviour. We shall first consider normal impact.

† For general references see: Johnson (1972) or Zukas & Nicholas (1982).

‡ Since we are concerned here with normal impact only the suffix z will be omitted.

https://doi.org/10.1017/CBO9781139171731.012 Published online by Cambridge University Press

Up to the instant of maximum compression the kinetic energy is absorbed in local deformation, elastic and plastic, of the two colliding bodies, i.e.

$$\tfrac{1}{2}mV^2 = W = \int_0^{\delta^*} P \, \mathrm{d}\delta \tag{11.40}$$

where $1/m = 1/m_1 + 1/m_2$ and V is the relative velocity of impact. After the point of maximum compression the kinetic energy of rebound is equal to the work done during elastic recovery, thus

$$\tfrac{1}{2}mV'^2 = W' = \int_0^{\delta^*} P' \, \mathrm{d}\delta' \tag{11.41}$$

where primed quantities refer to the rebound. We wish to determine the maximum contact stress, the duration of the impact and the 'coefficient of restitution' (V'/V) in terms of the impact velocity V and the properties of the two bodies. We shall restrict the discussion to spherical profiles, but the analysis may be extended to more general profiles without difficulty.

It is clear from equations (11.40) and (11.41) that the impact behaviour is determined by the compliance relation $P(\delta)$ for the contact, in both loading and unloading. These relationships under static conditions have been discussed in §§6.3 & 6.4 (see Fig. 6.17). In the elastic range ($P \leqslant P_Y$) loading and unloading are identical, expressed by equation (11.20). Yield initiates at a point beneath the surface and, as the plastic zone spreads, the mean contact pressure rises from $\sim 1.1Y$ to $\sim 3Y$ when the fully plastic condition is reached. Thereupon, in the absence of strain hardening, the contact pressure remains approximately constant, referred to as the flow pressure or yield pressure.

Unfortunately the compliance relationship for an elastic-plastic contact is not precisely defined, so that a theory of elastic-plastic impact is necessarily approximate. Since most impacts between metal bodies result in a fully plastic indentation we can concentrate on this regime. In our static analysis we assumed (*a*) that the total (elastic and plastic) compression δ was related to the contact size by: $\delta = a^2/2R$, i.e. neither 'pile-up' nor 'sinking in' occurs at the edge of the indentation, and (*b*) that the mean contact pressure p_m is constant and equal to $3.0Y$. These assumptions led to the compliance relation (6.41), which gives a fair prediction of the experimental results, as shown in Fig. 6.17. Making the same assumptions here and using equation (11.40) gives

$$\tfrac{1}{2}mV^2 = \int_0^{a^*} \pi a^2 p_d(a/R) \, \mathrm{d}a = \pi a^{*4} p_d / 4R \tag{11.42}$$

where p_d is used to denote the mean contact pressure during *dynamic* loading. We note that the quantity $\pi a^{*4}/4R$ is the apparent volume of material v_a displaced by an indenter of radius R. With a material which strain-hardens according

https://doi.org/10.1017/CBO9781139171731.012 Published online by Cambridge University Press

to a power law with index n (eq. (6.73)) it has been shown by Mok & Duffy (1965) that the right-hand side of equation (11.42) is multiplied by the factor $4n/(4n + 1)$ and p_d is the dynamic pressure at the instant of maximum compression.

Taking the rebound to be elastic, the energy of rebound W' is given by substituting equation (6.45) for the compliance relation into equation (11.41), where $P^*(=\pi a^{*2} p_d)$ is the compressive force between the bodies at the start of the rebound. Using equation (4.22) to eliminate the radii, the kinetic energy of rebound can be expressed in terms of the size of the indentation by

$$\tfrac{1}{2}mV'^2 = W' = \frac{3P^{*2}}{10a^*E^*} = \tfrac{3}{10}\pi^2 a^{*3} p_d{}^2/E^* \tag{11.43}$$

Eliminating a^* from equations (11.42 and 43) gives an expression for the coefficient of restitution:

$$e^2 \equiv \frac{V'^2}{V^2} = \frac{3\pi^{5/4}4^{3/4}}{10}\left(\frac{p_d}{E^*}\right)\left(\frac{\tfrac{1}{2}mV^2}{p_d R^3}\right)^{-1/4} \tag{11.44}$$

or, by writing $p_d \approx 3.0Y_d$ where Y_d is the dynamic yield strength,

$$e \approx 3.8(Y_d/E^*)^{1/2}(\tfrac{1}{2}mV^2/Y_d R^3)^{-1/8} \tag{11.45}$$

It is clear from this analysis that the coefficient of restitution is not a material property, but depends upon the severity of the impact. At sufficiently low velocities ($V < V_Y$ given by eq. (11.38)) the deformation is elastic and e is very nearly equal to unity. The coefficient of restitution gradually falls with increasing velocity. When a fully plastic indentation is obtained our theory suggests that e is proportional to $V^{-1/4}$. Some experimental results taken from Goldsmith (1960), shown in Fig. 11.11, illustrate this behaviour.

Fig. 11.11. Measurements of the coefficient of restitution of a steel ball on blocks of various materials (from Goldsmith, 1960). Cross – hard bronze; circle – brass; triangle – lead. Lines of slope $-\frac{1}{4}$.

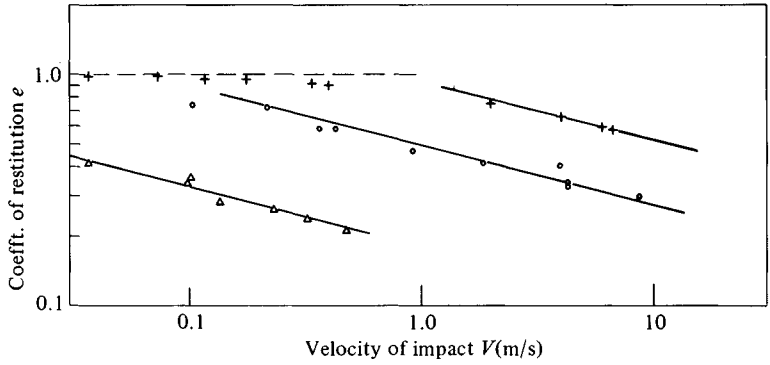

https://doi.org/10.1017/CBO9781139171731.012 Published online by Cambridge University Press

The coefficient of restitution is also very dependent upon the hardness of the material: according to equation (11.45) it is proportional to $Y_d^{5/8}$. Some experiments by Tabor (1948) with different materials are compared with equation (11.45) in Fig. 11.12. The general trend of the experiments follows the theory†, but the measured values of e are somewhat low.

Tabor (1948) and Crook (1952) used impact experiments to deduce the dynamic yield pressure p_d. As expected they found that the dynamic pressure was greater than the static yield pressure p_m by a factor which was somewhat larger for soft metals whose yield stress is sensitive to rate of strain (see Table 11.2). Furthermore it was found that the contact pressure does not remain constant throughout the period of plastic deformation, but falls, as the striker decelerates, to a value which is closer to the static pressure at the start of the rebound (denoted by p_r in Table 11.2). This fact accounts for the observed coefficients of restitution being lower than those predicted by the simple theory, which is based on the yield pressure being maintained constant up to the instant of closest approach.

Fig. 11.12. Variation of coefficient of restitution with dynamic hardness p_d. Solid circle – steel; triangle – Al alloy; square – brass; open circle – lead.

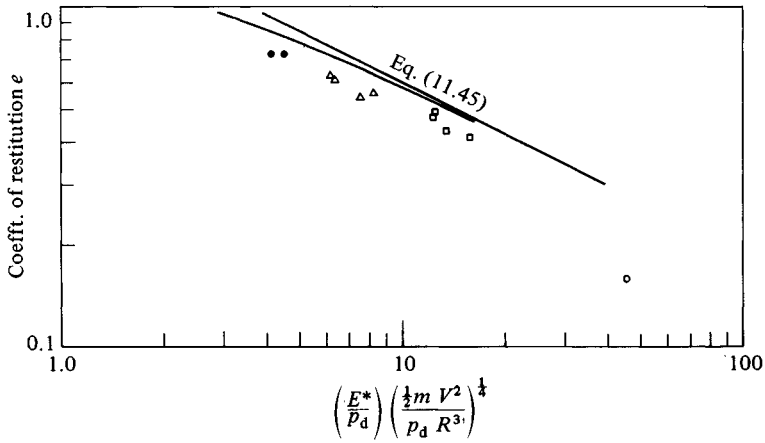

† Tabor (1948) develops a theory from a slightly different premise. Instead of taking $\delta = a^2/2R$, he assumes that the energy dissipated in plastic deformation $(W - W') = p_d v_r$, when v_r is the *residual* volume of the indentation after rebound. This assumption modifies equation (11.42) to read

$$\tfrac{1}{2}m(V^2 - \tfrac{3}{8}V'^2) = p_d v_a = \pi a^{*4} p_d / 4R \qquad (11.42a)$$

where V' is given by equation (11.43). The influence upon the coefficient of restitution is shown in Fig. 11.12.

https://doi.org/10.1017/CBO9781139171731.012 Published online by Cambridge University Press

The total time of impact is made up of two parts: the time of plastic indentation t_p and the time of elastic rebound t'. Making the same assumptions as before, that the flow pressure p_d is constant and that the compression $\delta = a^2/2R$, the indentation time may be easily calculated. The equation of relative motion of the two bodies is

$$m\frac{d^2\delta}{dt^2} = -\pi a^2 p_d = -2\pi R p_d \delta$$

where $1/m = 1/m_1 + 1/m_2$ and $1/R = 1/R_1 + 1/R_2$. The solution to this equation gives

$$t_p = \left(\frac{\pi m}{8Rp_d}\right)^{1/2} \tag{11.46}$$

which is independent of the velocity of impact. For a 10 mm diameter steel ball impinging on softer metals t_p has values in the range 10^{-4}-10^{-5} s. Assuming the rebound to be elastic and governed by the Hertz theory, the rebound time t' can be found from equations (11.45) and (11.24) with the result:

$$t' = 1.2et_p \tag{11.47}$$

where the coefficient of restitution e is given by (11.45) and t_p by (11.46). As the impact becomes more plastic, e falls and the rebound time t' becomes a smaller proportion of the total time of impact $(t_p + t')$.

During an oblique plastic impact friction forces between the projectile and the target are called into play and an elongated crater is produced. The oblique impact of a rigid sphere with a plastic solid has been analysed by Rickerby & Macmillan (1980) on very much the same basis as the theory of normal impact described above. The surface of the plastically deformed target is assumed to remain flat outside the crater and the penetration of the sphere is assumed to be resisted by a constant dynamic flow pressure p_d together with a frictional traction μp_d. Step-by-step calculations of the motion of the sphere, leading to the volume of the crater and the loss of kinetic energy of the projectile are well supported by experiment (Hutchings *et al.*, 1981)

Table 11.2

Metal	p_d/p_m	p_r/p_m
Steel	1.28	1.09
Brass	1.32	1.10
Al alloy	1.36	1.10
Lead	1.58	1.11

https://doi.org/10.1017/CBO9781139171731.012 Published online by Cambridge University Press

The simple theories of plastic impact outlined above are based on the assumption that the maximum penetration δ^* is given approximately by $a^{*2}/2R$. For this to be the case a^*/R must be less than about 0.5 so that, by equation (11.42), $(\frac{1}{2}mV^2/p_dR^3)$ must be less than about 0.05. For a steel sphere striking a steel surface this requires V to be less than 100 m/s.

(c) High speed impact

At higher speeds, associated with bullets and, in the extreme, with meteorites, the permanent deformation is much greater and the nature of the impact phenomenon changes in ways which depend upon the mechanical properties of both projectile and target. In addition, the energy dissipated during the impact produces a local temperature rise which can appreciably influence the material properties.

Johnson (1972) has suggested that the non-dimensional parameter $(\rho V^2/Y_d)$ provides a useful guide for measuring the regime of behaviour for the impact of metals. Table 11.3 is adapted from Johnson.

For illustrative purposes we shall consider the impact of a hard sphere of density ρ_1, impacting a massive block of density ρ and dynamic yield strength Y_d. Taking $p_d = 3Y_d$ the parameter $(\frac{1}{2}mV^2/p_dR^3)$ may then be written

$$\left(\frac{\frac{1}{2}mV^2}{p_dR^3}\right) = 0.72\left(\frac{\rho_1}{\rho}\right)\left(\frac{\rho V^2}{Y_d}\right) \approx \frac{\rho V^2}{Y_d}$$

since ρ_1/ρ is not going to differ much from unity compared with the variations in $(\rho V^2/Y_d)$ which appear in Table 11.3. For most metals the ratio of elastic modulus to yield stress E^*/Y_d is 100 or more, so that for purely elastic deformation, by equation (11.39), $(\rho V^2/Y_d)$ is generally less than 10^{-6}. When the elastic limit is first exceeded the plastic zone is contained beneath the surface, but fully plastic indentations are produced when the parameter (aE^*/Y_dR)

Table 11.3

Regime	$\rho V^2/Y_d$	Approx. velocity V (m/s)
Elastic	$<10^{-6}$	<0.1
Fully plastic indentation	$\sim 10^{-3}$	~ 5
Limits of shallow indentation theory	$\sim 10^{-1}$	~ 100
Extensive plastic flow, beginning of hydrodynamic behaviour	~ 10	$\sim 1\,000$
Hypervelocity impact	$\sim 10^3$	$\sim 10\,000$

https://doi.org/10.1017/CBO9781139171731.012 Published online by Cambridge University Press

exceeds about 30 (from Fig. 6.15), which corresponds to $(\rho V^2/Y_d) \approx 10^{-3}$. Between $(\rho V^2/Y_d) = 10^{-3}$ and 10^{-1} the impact is reasonably described by the quasi-static shallow indentation theory presented above. In the velocity range discussed so far heating effects are negligible.

A further increase in impact speed leads to more extensive plastic deformation. The plastic strains are large and shear heating reduces the dynamic yield strength of the material. If the projectile is hard compared with the target the crater diameter increases to more than that of the projectile and penetrations greater than one diameter are obtained. This is the typical range of bullet speeds. When $(\rho V^2/Y_d)$ approaches unity the nature of the deformation changes and can no longer be regarded as quasi-static. Under these circumstances the inertia stresses associated with the local plastic deformation are comparable in magnitude with the yield stress of the material which resists deformation. Inertia stresses become important in the plastically deforming zone because of the very high rates of strain which are occurring there. In the surrounding elastically deforming material inertia effects remain small. The parameter $(\rho V^2/Y_d)$ can be interpreted as the ratio of the 'stagnation pressure' of the moving projectile, conceived as a fluid jet, to the strength of the target in shear. When this ratio appreciably exceeds unity, the inertia of the deforming material becomes more important than its yield strength, so that it behaves more like an ideal fluid than a plastic solid. Theoretical analyses of high speed impact have been made on this basis by Bjork and others (see Kornhauser, 1964) with moderate success.

We now write

$$\frac{\rho V^2}{Y_d} = \left(\frac{E}{Y_d}\right)\left(\frac{\rho V^2}{E}\right) = \frac{E}{Y_d}\left(\frac{V}{c_0}\right)^2$$

Since E/Y_d is greater than 100, it is clear that $(\rho V^2/Y_d)$ will exceed unity and fluid-like behaviour will develop *before* (V/c_0) approaches unity and dynamic effects occur in the bulk of the solid. However when $(\rho V^2/Y_d)$ reaches values around 10^3, (V/c_0) approaches or exceeds unity, and the impact sets up intense shock waves in the material. This is the region of hypervelocity impact normally associated with meteorites and laser beams. The heat liberated may be sufficient to melt or vaporise some of the projectile and target. A fine curtain of spray is ejected from the crater at a speed in excess of the impact velocity. A larger shallow crater with a pronounced lip is produced; if the projectile is ductile, it mushrooms on impact and turns itself inside out. This behaviour has been reproduced by Johnson *et al.* (1968) using a plasticine projectile and target, whose low yield strength enables hypervelocity impact conditions to be obtained at a velocity less than 1000 m/s. For further information on hypervelocity impact the reader is referred to Kornhauser (1964).

(d) Impact of viscoelastic solids

So far in this section we have described the inelastic behaviour of materials in terms of plastic flow, characterised by a dynamic yield stress Y_d. This is appropriate for metals but it is not a good model for polymeric materials, including rubber, which are better described in terms of viscoelasticity. The quasi-static impact of a projectile with a linear viscoelastic solid can be analysed by the methods described briefly in §6.5.

Provided the energy dissipated at impact is a fairly small fraction α of the kinetic energy of impact, a rough and ready estimate of the coefficient of restitution may be made from measurements of the energy dissipated in a cyclic strain experiment whose period is comparable with the time of impact. It is usual to express the energy dissipation in cyclic strain by the loss tangent, $\tan\phi$, where ϕ is the phase angle between the cyclic stress and strain. The loading and unloading during impact correspond roughly to a half cycle, whereupon the coefficient of restitution is given by

$$e = (1-\alpha)^{1/2} = (1-\pi\tan\phi)^{1/2} \tag{11.48}$$

To take a specific example, a Maxwell material (defined in §6.5) strained at a frequency ω has a loss tangent $= 1/\omega T$, where T is the time constant of the material. If T_c is the time of impact, we can take ω as π/T_c, whereupon

$$e = (1-\alpha)^{1/2} \approx 1 - \tfrac{1}{2}\alpha = 1 - \tfrac{1}{2}(T_c/T) \tag{11.49}$$

provided that α is small, i.e. $T_c/T \ll 1$. Since the impact is predominantly elastic, T_c can be taken to be the elastic impact time given by equation (11.24).

In order to carry out a more exact analysis of a rigid sphere of mass m striking a viscoelastic half-space we have to make use of the results due to Ting (1966) outlined in §6.5. A general incompressible linear viscoelastic material has a creep compliance $\Phi(t)$ and a relaxation function $\Psi(t)$. Different equations govern the loading and unloading parts of the impact process. During loading ($0 < t < t^*$) the penetration $\delta(t)$ is related to the contact size $a(t)$ by the elastic equation:

$$\delta(t) = a^2(t)/R \tag{11.50}$$

The sphere retards under the action of the contact force $P(t)$, which from equation (6.60) is given by

$$-m\ddot{\delta}(t) = P(t) = \frac{8}{3R}\int_0^t \Psi(t-t')\,\frac{\mathrm{d}}{\mathrm{d}t'}a^3(t')\,\mathrm{d}t' \tag{11.51}$$

The variation of force and penetration with time during loading are obtained by the simultaneous solution of equations (11.50) and (11.51). The maximum contact size coincides with the maximum penetration when $t = t^*$.

During the rebound ($t > t^*$), $a(t)$ is decreasing, whereupon $P(t)$ and $\delta(t)$ depend upon the time t_1 during loading, at which the contact size $a(t_1)$ was

https://doi.org/10.1017/CBO9781139171731.012 Published online by Cambridge University Press

equal to the current contact size $a(t)$. The penetration is given by

$$\delta(t) = a^2(t)/R - \int_{t^*}^{t} \Phi(t-t') \frac{\mathrm{d}}{\mathrm{d}t'} \left[\int_{t_1}^{t'} \Psi(t'-t'') \frac{\mathrm{d}}{\mathrm{d}t''} \{a^2(t'')\} \, \mathrm{d}t'' \right] \mathrm{d}t' \quad (11.52)$$

and the contact force by

$$-m\ddot{\delta}(t) = P(t) = \frac{8}{3R} \int_0^{t_1} \Psi(t-t') \frac{\mathrm{d}}{\mathrm{d}t'} a^3(t') \, \mathrm{d}t' \quad (11.53)$$

The simultaneous solution to equations (11.52) and (11.53) gives the variation of force and displacement during the rebound.

A solution in closed form to these equations has been obtained by Hunter (1960) for the simple case of a Maxwell material in which the dissipation is small (i.e. in which the time of impact T_c is short compared with the relaxation time T of the material). The coefficient of restitution was found to be given by

$$e \approx 1 - (4/9)(T_c/T) \quad (11.54)$$

This result is very close to the approximate value obtained in equation (11.49) from the energy loss in cyclic strain.

For more complex materials, or when T_c/T is no longer small, equations (11.50)–(11.53) must be solved numerically step by step. This has been done by Calvit (1967) using creep and relaxation functions estimated from cyclic strain tests on perspex. Values of the coefficient of restitution and the time of impact obtained by experiment were both found to be somewhat lower than calculated.

11.6 Travelling loads - high speed sliding and rolling

In the discussion of sliding and rolling contact in Chapters 7 and 8 it was assumed that the velocity of the point of contact over the surface was sufficiently slow for the deformation to be quasi-static. This is true for most engineering purposes but, if the velocity approaches the speeds of elastic wave propagation, the inertia of the material plays a part and modifies the contact stresses. By analogy with a body moving through a fluid, we can identify three regimes: 'subsonic', 'transonic' and 'supersonic'† depending upon the ratio of the velocity to the elastic wave speed. On the surface of an elastic solid the behaviour is complicated by the fact that there are three wave speeds involved: dilatational c_1, shear c_2 and surface c_3. In this section we shall merely outline

† Referred to by some authors as 'subseismic', etc.

https://doi.org/10.1017/CBO9781139171731.012 Published online by Cambridge University Press

the main features of the dynamic effects for two-dimensional deformation (plane strain) only.†

(a) Moving line load on an elastic half-space

The fundamental problem concerns the stresses and deformation set up in an elastic half-space by a concentrated line force P per unit length moving with velocity V over the surface. It is the dynamic equivalent of the static problem considered in §2.2. An analysis using the complex variable method, which covers the subsonic, transonic and supersonic regimes, has been made by Cole & Huth (1958). They only investigate steady-state solutions, for which an Eulerian coordinate system which moves with the load can be used. Mach numbers M_1 and M_2 are defined as

$$M_1 = V/c_1 \quad \text{and} \quad M_2 = V/c_2$$

Under 'subsonic' conditions, when M_1 and $M_2 < 1$, we define:

$$\beta_1 = (1 - M_1^2)^{1/2}, \quad \beta_2 = (1 - M_2^2)^{1/2}$$

and

$$N = (2 - M_2^2)^2 - 4\beta_1\beta_2$$

Cole & Huth show that the surface displacement $\bar{u}_z$ at a point distance x from the load is given by

$$\bar{u}_z = \frac{2(1+\nu)P}{\pi E} \frac{\beta_1 M_2^2}{N} \ln|x| + C \tag{11.55}$$

where C is a constant determined by the choice of the datum for displacements.

At low velocity, $V \to 0, \beta_1 \to 1$ and $N \to 2(M_1^2 - M_2^2) = -M_2^2/(1-\nu)$. Thus the expression for the surface displacement reduces to

$$\bar{u}_z = -\frac{2(1-\nu^2)P}{\pi E} \ln|x| + C \tag{11.56}$$

which is the static result obtained in equation (2.19). With an increase in velocity the logarithmic shape of the surface remains unchanged, but the magnitude of the displacement increases by the factor $\{\beta_1 M_2^2/(1-\nu)N\}$ approaching an infinite value as N approaches zero. Reference to equation (11.7) will confirm that this situation arises when the velocity V coincides with the speed c_3 of Rayleigh surface waves. Then $M_2 = \alpha$ and $M_1 = \alpha c_2/c_1$. It is not surprising that an undulation which travels freely along the surface at speed c_3 increases without limit if forced by a load moving at the same speed. Cole & Huth have obtained expressions for the stress components beneath

† The three-dimensional problem of a moving point force on an elastic half-space has been considered by Eason (1965).

https://doi.org/10.1017/CBO9781139171731.012 Published online by Cambridge University Press

the surface as a function of the speed and elastic properties of the surface. The distributions of normal stress $\sigma_z(x)$ along a line at depth z for $M_2 = 0$, 0.5 and 0.9 are shown in Fig. 11.13. The amplification of the stress with speed as V approaches $c_3 (M_2 \to 0.93)$ is clearly shown, but for $M_2 < 0.5$ the difference from the static stress distribution is small. At high subsonic speeds the normal acceleration $\ddot{u}_z$ leads to the stress σ_z becoming tensile at some distance on either side of the load. In the subsonic regime the normal surface displacements are symmetrical ahead of and behind the load so that no net work is done by the moving load.

If we turn now to the completely 'supersonic' case where V is greater than the largest of the wave speeds, then both M_1 and $M_2 > 1$. We now write

$$\beta_1' = (M_1^2 - 1)^{1/2}, \quad \beta_2' = (M_2^2 - 1)^{1/2}$$

and

$$N' = (2 - M_2^2) + 4\beta_1'\beta_2'$$

The solution for the displacements and stresses is completely different from the 'subsonic' case. The surface displacement may be written

$$\bar{u}_z = \begin{cases} 0, & x < 0 \\ \dfrac{2(1+\nu)P}{E} \dfrac{\beta_1' M_2^2}{N'}, & x > 0 \end{cases} \tag{11.57}$$

Ahead of the load the surface is undisturbed; behind the load, it is uniformly depressed by an amount which depends upon the speed. The stresses in the half-space are zero everywhere except along the lines of two 'shock waves' propagating from the point of application of the load. At the wave front the stress is theoretically infinite. The shock waves travel at velocities c_1 and c_2

Fig. 11.13. Normal stress σ_z due to a line load P moving subsonically ($V < c_2$) over the surface of an elastic half-space, for $M_2 = 0$, 0.5 and 0.9. ($\nu = \frac{1}{3}$, $M_2/M_1 = 2$.)

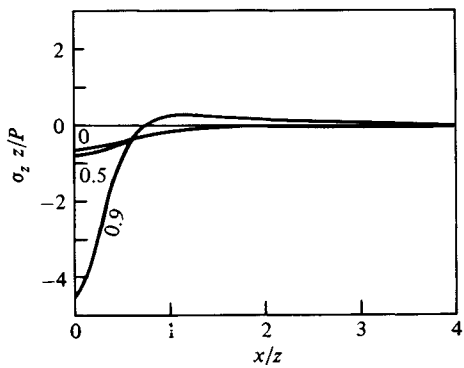

https://doi.org/10.1017/CBO9781139171731.012 Published online by Cambridge University Press

and hence make angles of $\cot^{-1}(\beta_1')$ and $\cot^{-1}(\beta_2')$ with the surface as shown in Fig. 11.14. This process is no longer conservative; the moving load does work as it permanently depresses the surface and strain energy is steadily radiated away by the shock waves.

The 'transonic' regime is complicated. In the small range of speed $c_3 < V < c_1$, N changes sign so that a downward force on the surface gives rise to an upward displacement in the vicinity of the force. For $c_2 < V < c_1$, N is complex and the stresses and deformation are a combination of a shock wave travelling at speed c_2 and a 'subsonic' pattern associated with c_1. For details consult Cole & Huth (1958).

(b) High speed rolling or sliding of a cylinder

We shall now consider the stresses and deformation set up by a long rigid, frictionless cylinder which slides or rolls over the surface of an elastic half-space with velocity V perpendicular to its axis (Craggs & Roberts, 1967). We have seen that in the 'subsonic' regime the deformation of the surface by a moving line load is similar in shape to that produced by a stationary load; the dynamic effect is to amplify the displacements by the speed factor $\{\beta_1 M_2^2/(1-\nu)N\}$ where β_1, M_2 and N are defined above. Thus the half-space deforms as though its rigidity were reduced by the same factor. Now the contact pressure distribution with the moving cylinder can be built up by the superposition of concentrated loads, such that the resultant deformation in the contact zone matches the profile of the cylinder. It follows that the pressure distribution will be similar to the static (Hertz) case, and the contact width will be increased by:

$$a(V) = a(0)\{\beta_1 M_2^2/(1-\nu)N\}^{1/2} = \left\{\frac{4(1+\nu)PR}{\pi E}\,\frac{\beta_1 M_2^2}{N}\right\}^{1/2} \qquad (11.58)$$

Fig. 11.14. Line load moving supersonically ($V > c_1$) over the surface of an elastic half-space showing shock waves. ($\nu = 0.25$.)

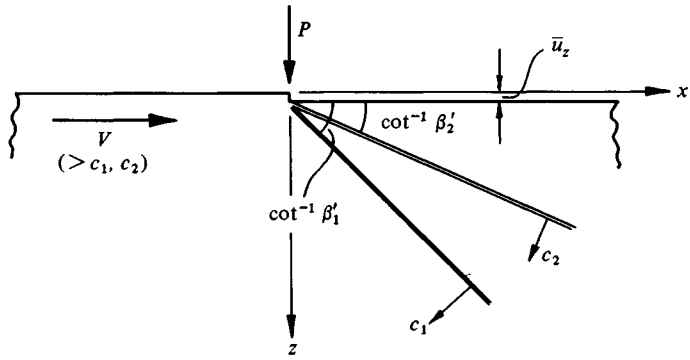

https://doi.org/10.1017/CBO9781139171731.012 Published online by Cambridge University Press

For a given load P, therefore, the maximum contact pressure $p_0(V)$ is reduced by the same factor. It is clear from Fig. 11.13 that the subsurface stresses do not follow a distribution which is similar to the static case. They may be deduced from the results given by Craggs & Roberts (1967).

It is immediately apparent from equation (11.58) that the indentation of the half-space by the cylinder becomes excessively large when V approaches the Rayleigh wave speed ($N \to 0$). Above the Rayleigh wave speed ($c_3 < V < c_2$) the change in sign of the surface displacements makes it impossible for the cylinder to make contact with the surface of the half-space along a continuous arc. In fact no physically acceptable steady-state solution appears to exist in the range $c_3 < V < c_1$ (Craggs & Roberts, 1967).

In the 'supersonic' regime ($V > c_1$), however, a simple solution can be found from the results for a line load. The surface is undisturbed until it meets the cylinder at $x = -a$. By equation (11.57) each increment of pressure $p\ \mathrm{d}x$ depresses the surface by an amount

$$\mathrm{d}\bar{u}_z = \frac{2(1+\nu)}{E}\ \frac{\beta_1' M_2^2}{N'}\ p\ \mathrm{d}x$$

Thus the pressure is proportional to the slope of the profile $\mathrm{d}\bar{u}_z/\mathrm{d}x$, which is triangular. The surface leaves the cylinder at its lowest point at a depth d given by

$$d = \frac{a^2}{2R} = \frac{2(1+\nu)P}{E}\ \frac{\beta_1' M_2^2}{N'} \tag{11.59}$$

as shown in Fig. 11.15. Trains of stress waves are propagated from the arc of contact at velocities c_1 and c_2.

Fig. 11.15. Frictionless cylinder rolling or sliding supersonically ($V > c_1$) over the surface of an elastic half-space.

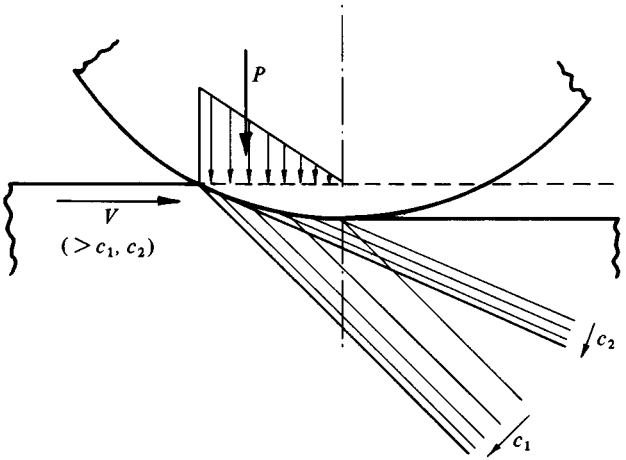

https://doi.org/10.1017/CBO9781139171731.012 Published online by Cambridge University Press